HHS Public Access

Author manuscript

Radiother Oncol. Author manuscript; available in PMC 2022 April 01.

Published in final edited form as:

Radiother Oncol. 2021 April ; 157: 155–162. doi:10.1016/j.radonc.2021.01.023.

Characterization of cardiovascular injury in mice following partial-heart irradiation with clinically relevant dose and fractionation

Chang-Lung Lee[1,2,#], **Jessica W. Lee**[1,#], **Andrea R. Daniel**[1], **Matt Holbrook**[3], **Stephanie Hasapis**[1], **Ato O. Wright**[1], **Jeremy Brownstein**[1,6], **Lorraine Da Silva Campos**[1], **Yan Ma**[1], **Lan Mao**[4], **Dennis M. Abraham**[4], **Cristian T. Badea**[3], **David G. Kirsch**[1,5,*]

[1]Department of Radiation Oncology, Duke University Medical Center, Durham, North Carolina 27710, USA.

[2]Department of Pathology, Duke University Medical Center, Durham, North Carolina 27710, USA.

[3]Center for In Vivo Microscopy, Department of Radiology, Duke University Medical Center, Durham, North Carolina 27710, USA.

[4]Divison of Cardiology, Department of Medicine, Duke University Medical Center, Durham, North Carolina 27710, USA.

[5]Department of Pharmacology & Cancer Biology Duke University Medical Center, Durham, North Carolina 27710, USA.

[6]Current affiliation: Department of Radiation Oncology, Arthur G. James Comprehensive Cancer Center and Richard J. Solove Research Institute, The Ohio State University Medical Center, Columbus, Ohio 43210, USA.

Abstract

Background and purpose—Late cardiac toxicity is a major side effect of radiation therapy (RT) for breast cancer. We developed and characterized a mouse model of radiation-induced heart disease that mimics the dose, fractionation, and beam arrangement of left breast and chest wall RT.

Material and methods—Female wild-type (C57BL6/J) and atherosclerosis-prone apolipoprotein E-deficient ($ApoE^{-/-}$) mice (on a C57BL/6J background) on regular chow were treated with 2 Gy × 25 fractions of partial-heart irradiation via opposed tangential beams to the left chest wall. The changes in myocardial perfusion and cardiac function of C57BL/6J mice were examined by single-photon emission computed tomography (SPECT) and echocardiography, respectively. In addition to SPECT and echocardiography, the formation of calcified plaques and changes in cardiac function of $ApoE^{-/-}$ mice were examined by dual-energy microCT (DE-CT) and pressure-volume (PV) loop analysis, respectively. The development of myocardial fibrosis was examined by histopathology.

*CORRESPONDENCE David G. Kirsch, Duke University Medical Center, Box 91006, Durham, NC 27708, Phone: 919-681-8605, Fax: 919-681-1867, david.kirsch@duke.edu.

#These authors contribute equally to this work.

Results—Compared to unirradiated controls, irradiated C57BL/6J mice showed no significant changes by SPECT or echocardiography up to 18 months after 2 Gy × 25 partial-heart irradiation even though irradiated mice exhibited a modest increase in myocardial fibrosis. For ApoE$^{-/-}$ mice, 2 Gy × 25 partial-heart irradiation did not cause significant changes by SPECT, DE-CT, or echocardiography. However, PV loop analysis revealed a significant decrease in load-dependent systolic and diastolic function measures including cardiac output, dV/dtmax and dV/dt min 12 months after RT.

Conclusions—Following clinically relevant doses of partial-heart irradiation in C57BL/6J and ApoE$^{-/-}$ mice, assessment with noninvasive imaging modalities such as echocardiography, SPECT, and DE-CT yielded no evidence of decreased myocardial perfusion and cardiac dysfunction related to RT. However, invasive hemodynamic assessment with PV loop analysis indicated subtle, but significant, changes in cardiac function of irradiated ApoE$^{-/-}$ mice. PV loop analysis may be useful for future preclinical studies of radiation-induced heart disease, especially if subtle changes in cardiac function are expected.

Keywords

Radiotherapy; Cardiotoxicity; Radiobiology; Apolipoproteins E; Echocardiography; Tomography; Emission-Computed; Single-Photon; Hemodynamics; Mice; Inbred C57BL; Radiation-Induced Abnormalities

INTRODUCTION

Radiation-induced heart disease (RIHD) is a major late side effect of radiation therapy (RT) for breast cancer and other thoracic cancers. Many women who have been treated with adjuvant RT for left-sided breast cancer received 2 Gy daily fractions to 50 Gy total. While adjuvant RT improves overall survival in patients with invasive breast cancer, survivors who receive RT are at increased risk of late cardiac morbidity and mortality (1–4). A population-based study of 2,168 women receiving RT for breast cancer reported that each 1 Gy increase in mean heart dose conferred a 7.4% increase in the risk of major coronary events, without an apparent threshold (4). Cardiac doses and risk of RIHD are higher in women with left-sided breast cancers, given the increased proximity to the heart. Another study of women receiving breast conservation treatment estimated a cumulative risk of cardiac death 20 years following RT of 6.4% vs. 3.6% in left-sided vs. right-sided patients (3).

Recent preclinical rodent models of RIHD have shown that a single fraction of 15–20 Gy to the whole heart results in reduced microvascular endothelial density and function, increased von Willebrand factor deposition, increased mast cells and CD45-positive inflammatory cells, increased mitochondrial permeability, as well as sub-endocardial and myocardial fibrosis (5–9). Single fraction whole-heart RT also results in functional impairment. Seemann et al. reported modest decreases in end-systolic and end-diastolic volumes and increased ejection fraction by ultrasound and single photon emission computed tomography (SPECT) at 20–40 weeks after a single 2–16 Gy fraction in C57BL/6J mice (10). The same group also characterized atherosclerosis-prone *ApoE*$^{-/-}$ mice, which had more

myocardial fibrosis and inflammatory plaques compared to the C57BL/6J mice, but still only demonstrated modest decreases in cardiac function after RT (11).

The vast majority of preclinical models have utilized whole-heart RT delivered in a single or limited number of fractions. However, adjuvant RT following breast conserving surgery or mastectomy typically only affects part of the heart and is traditionally delivered in 1.8–2 Gy daily fractions for several weeks. We previously developed a RT plan using opposed tangential beams that include the anterior left ventricle, which more closely mimics plans treating the left breast or chest wall (12). Using dual-energy and 4D micro computed tomography (CT) and SPECT, we found decreased ejection fraction following a single 12 Gy fraction of partial-heart RT in radiosensitive *Tie2Cre; p53*$^{FL/-}$ mice compared to their heterozygous counterparts (12).

Here, we aimed to study cardiovascular injury in C57BL/6J and atherosclerosis-prone *ApoE*$^{-/-}$ female mice following fractionated partial-heart RT, with 2 Gy daily fractions to 50 Gy delivered via opposed tangential beams, similar to what breast cancer survivors have received. The changes in cardiac function and physiology after partial-heart irradiation were characterized using noninvasive imaging modalities including SPECT, dual-energy source CT (DE-CT) and echocardiography as well as invasive pressure-volume (PV) loop analysis.

MATERIALS AND METHODS

Mice.

All animal procedures were approved by the Institutional Animal Care and Use Committee at Duke University. Eight to ten-week old female C57BL/6J (JAX ID: 000664) and ApoE$^{-/-}$ mice on a C57BL/6J background (JAX ID: 002052) fed a regular diet (LabDiet 5058) were used for irradiation experiments. Age-matched female mice with the same genetic background and diet were used as unirradiated controls. Only female mice were used in the study because this project was aimed to model cardiac function in breast cancer patients treated with radiation therapy. Irradiated C57BL/6J mice and unirradiated controls were assessed at 3, 9, and 18 months after partial heart irradiation. Irradiated ApoE$^{-/-}$ mice and unirradiated controls were assessed at 3, 6, and 12 months after partial heart irradiation because this strain is known to develop accelerated radiation-induced heart disease (11, 13).

Radiation.

Partial-heart irradiation was delivered using a small animal irradiator, X-RAD 225Cx (Precision X-Ray). Irradiated mice received 2 Gy daily fractions Monday - Friday to a total dose of 50 Gy. Before each treatment, mice were anesthetized with isoflurane, positioned prone on the treatment stage, and aligned using onboard fluoroscopic image guidance using 40 kVp (2.5 mA) X-rays and a 2 mm Al imaging filter. Unirradiated control mice did not receive anesthesia.

To model cardiac exposure to radiation in patients treated with adjuvant RT for left-sided breast cancer, we used the same dose-fractionation with opposed tangential beams covering the anterior left ventricle (Figure 1, A and B). With the gantry rotated to the right anterior oblique (RAO) position at 225 degrees, the isocenter was set at 6–8 mm cranial to the dome

of the diaphragm and 2 mm anterior to the sternum (Figure 1A). Treatments were delivered using 225 kVp (13 mA) X-rays with a 3 mm Cu treatment filter. Treatment beams were collimated with a Cu portal, yielding a 10 × 10 mm square field with a dose rate of 4 cGy/sec at isocenter. The dose rate was measured with an ion chamber by members of the Radiation Safety Division at Duke University. Equally weight and opposed left posterior oblique (LPO, 45 degrees) and right anterior oblique (RAO, 225 degrees) fields were used with the isocenter defined above. The treated volume included the anterior left ventricle and anterior intraventricular septum, and excluded most of the right ventricle, as shown in a representative treatment plans in Figure 1B. Heart and lung volumes were also contoured on a representative CT, and a representative dose-volume histogram is shown in Supplemental Figure 1A. In a representative sample of four mice, the mean heart dose was 38.5 ± 1.0 Gy, and the mean lung dose was 10.4 ± 1.1 Gy, as shown in Supplemental Figure 1B.

Histologic analyses.

Mice were euthanized by CO_2 asphyxiation according to the recommended procedures of the Division of Laboratory Animal Resources at Duke University, and in a manner acceptable to the American Veterinary Medical Association. Whole-heart samples were embedded in paraffin as previously described (14). H&E-stained heart sections from all mice were examined for the presence of myocardial degeneration and necrosis by a single observer blinded to the genotype (C-L.L.). To assess cardiac fibrosis, Sirius red staining was used to visualize fibrosis and was performed using the VitroView Picro-Sirius Red Stain Kit (VitroVivo Biotech) according to the manufacturer's instructions. Three sections per mouse heart were taken in order to include sections from the base, mid, and apex of the left ventricle, and images were acquired at 1.25x magnification in order to capture the entire section. An in-house MATLAB image segmentation script was used to measure the total area of each cardiac section and the area of each cardiac section staining red, which indicated fibrosis; visible large vessels were excluded. The percent of fibrosis per section was averaged across multiple sections for the same mouse.

Echocardiography.

Echocardiography was obtained on conscious mice without anesthesia from all groups with a Vevo 2100 high-resolution imaging system (VisualSonics) as previously described (15). Echocardiography data were read by two observers (L.M. and D.A.) blinded to treatment.

Dual-energy CT and 4D-CT.

Dual-energy microCT (DE-CT) and 4D-CTwas performed using a system developed in the Center for In Vivo Microscopy at Duke University. The acquisition technique has been described previously (12). Briefly, mice were first injected intravenously with 0.004 mL/g Au nanoparticle contrast (AuroVist), which takes a few days to accumulate in injured tissue. 3 days later, mice were intravenously injected with 0.012 mL/g liposomal iodine, then DE-CT was immediately performed followed by a 4D-microCT acquisition. Each animal was anesthetized with isoflurane (1.5%) mixed with 50% oxygen and balanced with nitrogen. ECG was monitored with electrodes taped to the footpads, and body temperature was maintained with heat lamps, a rectal probe, and feedback controller. A pneumatic pillow on the thorax was used to monitor respiration. DE-CT enabled both dual energy decomposition

to quantify the calcified plaques and possible accumulation of Au nanoparticles in the injured myocardium, while data from 4D-CT were utilized to assess global function of the left ventricle. Data analyses were performed using ITK snap (http://www.itksnap.org/) by a single observer blinded to treatment (S.H.).

SPECT.

MicroSPECT acquisitions were performed with a U-SPECTII/CT system fitted with a 0.35 mm multi-pinhole collimator (MILabs, Utrecht, Netherlands) according to previously described methods (12). Reconstructed images were analyzed by a single observer blinded to treatment (C-L.L.).

Pressure-volume loop analysis.

In vivo pressure-volume (P-V) analysis was performed as previously described (16, 17). Briefly, mice were anesthetized with ketamine (100 mg/kg) and xylazine (2.5 mg/kg) and underwent endotracheal intubation with mechanical ventilation. After bilateral vagotomy, the chest was opened and the pericardium was dissected to expose the heart. A 1.4 French pressure-conductance catheter (Millar Instruments, Houston, TX) was inserted retroaortically into the LV to record hemodynamics. Baseline hemodynamic parameters were obtained once the catheter recordings had achieved steady state, usually 3–5 minutes following conductance catheter placement. A 7–0 suture ligature was placed around the inferior vena cava (IVC) to manipulate preload. Subsequently, parallel conductance (Vp) was determined by 10 μL injection of 15% saline into the right jugular vein to establish the parallel conductance of the blood pool. The derived Vp was used to correct the P-V loop data. Data were recorded digitally at 1,000 Hz and analyzed with pressure volume analysis software (PVAN data analysis software version 3.3; Millar Instruments) as previously described (15). After PV loops, mice were euthanized by cervical dislocation under anesthesia to collect the hearts for histology. PV loop data were read by two observers (L.M. and D.A.) blinded to treatment.

Statistics.

Histology, imaging, and PV loop parameters between unirradiated and irradiated mice were compared via two-tailed Mann-Whitney U test, and significance was assumed if $p<0.05$. Data are presented as mean +/− standard error of the mean (SEM) Calculations were performed using GraphPad Prism 8 (GraphPad Software, Inc).

RESULTS

We irradiated female C57BL/6J mice with 25 fractions of 2 Gy partial-heart irradiation and included C57BL/6J littermates that were not irradiated as controls. These mice were scanned with micro-SPECT to assess cardiac perfusion at 3, 9 and 18 months after irradiation. In addition, transthoracic echocardiography and histology analysis was conducted 18 months after irradiation. Longitudinal SPECT scans did not demonstrate a measurable decrease in regional cardiac perfusion up to 18 months post-irradiation (Figure 2A). Examination of tissue sections from the myocardium of unirradiated and irradiated mice did not reveal the presence of myocardial degeneration and necrosis (data

not shown), although Sirius red staining revealed a modest, but significant, increase in left ventricular fibrosis at 18 months in irradiated mice (Figure 2B). In addition, evaluation of left ventricular function by echocardiographic measurements 18 months after irradiation showed no statistically significant differences in fractional shortening (FS), left ventricular end-diastolic diameter (LVDd) and left ventricular end-systolic diameter (LVDs) between irradiated and unirradiated mice (Figure 2, C to E and Supplementary Table 1). Together, these results suggest that while 2 Gy × 25 partial-heart irradiation may lead to subtle increases in myocardial fibrosis, ultimately there were no detectable impairments in vascular permeability and cardiac function of C57BL/6J mice up to 18 months after irradiation.

ApoE$^{-/-}$ mice are prone to atherosclerosis, which is a major mechanism of coronary artery disease that is accelerated by radiation therapy (18). Previous reports demonstrated that male mice lacking ApoE develop microvascular damage, coronary atherosclerosis, and decreased survival following whole-heart irradiation (11, 13). We irradiated female ApoE$^{-/-}$ mice with 25 fractions of 2 Gy partial-heart irradiation and also evaluated unirradiated littermate controls. SPECT scans did not show detectable changes in myocardial perfusion in both irradiated and unirradiated mice 3 and 6 months after irradiation (**data not shown**). In addition to SPECT, we also performed DE-CT with Au nanoparticle and liposomal iodine contrast agents to assess cardiac function (12) and the number of calcified plaques of the heart (19, 20). While the number of calcified plaques increased over time across all ApoE$^{-/-}$ mice, no significant difference in calcified plaques was detected between the irradiated and control mice (Figure 3, A–D). In addition, DE-CT data did not show cardiac Au nanoparticle contrast extravasation or accumulation in the irradiated or control mice (**data not shown**). Cardiac function analysis using 4D-CT also did not show significant differences in ejection fraction or stroke volume between the irradiated and control mice at 3 and 6 months (Figure 3, E–F). Similarly, echocardiogram parameters including fractional shortening, LVDd and LVDs were not significantly different between the irradiated and control mice at 12 months (Figure 4A and Supplemental Table 2). Sirius red staining for fibrosis showed a slight trend towards increased fibrosis in the irradiated mice, although the difference was not statistically significant (Supplemental Figure 2).

To investigate whether irradiation altered load independent measures of cardiac contractility and compliance, we also performed pressure-volume (PV) loop analysis 12 months after radiation (17). Baseline measurements at 12 months in irradiated and control ApoE$^{-/-}$ mice are shown in Supplemental Table 3. Maximum volume (Vmax), which approximates end-diastolic volume, was significantly lower in irradiated vs. control mice. Irradiation also induced systolic dysfunction, as measured by cardiac output (CO) (Figure 4B) and corresponding trends toward reduced stroke volume (SV), first derivative of pressure with respect to time (dP/dt max), and stroke work (SW) in irradiated ApoE$^{-/-}$ mice. Additionally, irradiation impaired early diastole or active relaxation with significantly lower magnitude of dV/dt min, the greatest decrease in ventricular volume with respect to time (Figure 4C). Load-independent compliance and contractility parameters, obtained by IVC constriction in PV loop analysis, are shown in Supplemental Table 4. The linear slope of the end-diastolic pressure volume relationship (EDPVR) and the quadratic β (stiffness) coefficient trended higher in irradiated mice, suggesting decreased compliance or increased ventricular stiffness,

but no significant differences were seen. The linear slope of the end-systolic pressure volume relationship (ESPVR) or end-systolic elastance and the peak elastance (Emax) and preload recruitable stroke work (PRSW) trended lower in the irradiated mice, suggesting decreased contractility. In sum, invasive hemodynamics suggest that 50 Gy partial-heart irradiation delivered in 25 fractions to $ApoE^{-/-}$ mice induces subtle impairments in load dependent measures of systolic and diastolic performance.

DISCUSSION

In this study, we used a clinically relevant mouse model of 2 Gy × 25 fractions to the left breast/chest wall, which included the anterior LV and septum, to model RIHD in breast cancer survivors (Figure 1). We followed female C57BL/6J mice up to 18 months after RT to capture late side effects. SPECT and echocardiography showed no significant differences in the irradiated and unirradiated mice (Figure 2). In contrast, a previous study by Seemann et al. with similarly aged male C57BL/6J mice also on a regular diet reported modest reductions of 10–39% in end-diastolic and end-systolic volume and increases of 20% in ejection fraction by SPECT at 20–40 weeks following a single 8–16 Gy fraction to the entire heart (10). This phenotype may be due to the large fraction size and volume irradiated. Like other normal tissues, the heart has a low a/b ratio, with 1.8–2.8 estimated for the capillary component, making it more sensitive to large fraction sizes (21). For comparison, the equivalent dose in 2 Gy fractions (EQD2) of 8 and 16 Gy single fractions are 20 Gy and 72 Gy, respectively. While an EQD2 of 20 Gy is lower than the 50 Gy used in the present study, it is possible that the onset of myocardial dysfunction would be delayed when only part of the myocardium was irradiated because the unirradiated myocardium might have been able to functionally compensate for injured myocardium within the irradiated field. For example, we observed compensated myocyte hypertrophy in the unirradiated myocardium of radiosensitive *Tie2Cre; $p53^{FL/-}$* mice treated with a single dose of 12 Gy partial-heart irradiation (12). In addition, the formation of heart failure after 12 Gy whole-heart irradiation was substantially delayed in *VECre; $p53^{FL/-}$* mice, in which only a subset of endothelial cells were sensitized to radiation, compared to *Tie2Cre; $p53^{FL/-}$* mice, in which all endothelial cells in the heart were sensitized to radiation (14). Overall, the contrast in findings following a single fraction of whole heart irradiation and the present study with fractionated partial-heart irradiation emphasizes the importance of selecting and accurately reporting dose-volume experimental parameters (22).

Our previous studies using genetically engineered mice where endothelial cells are sensitized to radiation demonstrate substantial vascular damage and myocardial necrosis after 12 Gy or 3 Gy × 10 whole-heart irradiation as well as 12 Gy partial-heart irradiation. Seemann et al. also reported that single doses 8 to 16 Gy whole heart radiation in C57BL/6J mice result in epicardial inflammation and microvascular injury, which contribute to albumin leakage, amyloid formation and increased collagen deposition in the left ventricle measured by Sirius red staining (10). In addition, it has been shown that a single dose of 8 Gy irradiation causes persistently elevated expression of inflammatory markers ICAM-1 and VCAM-1 on cardiac endothelial cells (23). Although tissues samples from early time points after irradiation are not available in the present study, our results from Sirius red staining show a modest increase in myocardial fibrosis in C57BL/6J mice 18 months after 2 Gy × 25

partial-heart irradiation. However, longitudinal SPECT scans do not show detectable defects in myocardial perfusion up to 18 months after irradiation (Figure 2). Thus, our findings suggest that 2 Gy × 25 partial-heart irradiation may result in less profound vascular injury in C57BL/6J mice compared to whole-heart irradiation with higher doses per fraction.

As wild-type mice are generally resistant to atherosclerosis, which is one process that can increase the risk of RIHD, we also examined atherogenic ApoE$^{-/-}$ mice fed a regular diet (24, 25). Our data did not show any significant differences in calcified plaques or cardiac function between unirradiated and irradiated ApoE$^{-/-}$ mice using noninvasive imaging methods including dual-energy CT and echocardiography (Figure 3 and 4A). While there was an increase in collagen deposition in the irradiated mice as 12 months, the increase was not statistically significant (Supplemental Figure 2). Gold-standard hemodynamic assessment with PV loop analysis revealed reductions in chamber dimensions (Ved), systolic function (CO, dV/dt max), and diastolic function (dV/dt min) in irradiated vs. control ApoE$^{-/-}$ mice. Other parameters including Ves, SV, and SW also trended downwards while EF trended upwards post-RT, though changes were not significant likely due to the limited sample size (Figure 4, B–C). Similar changes in cardiac chamber dimensions were also observed a prior study of ApoE$^{-/-}$ mice on a regular diet receiving a single 16 Gy fraction to the entire heart. Gabriels et al. reported subtle decreases in Ved and Ves and increases in EF, though these changes were apparent by echocardiography and SPECT at 20 weeks (11). Unlike the present study, Gabriels et al. did identify significant increases in coronary artery plaques and collagen deposition after 16 Gy, although the absolute increases were low. For example, after 40 weeks, interstitial collagen deposition was approximately 0.4% of total tissue area in the control mice and 1.8% in the 16 Gy mice, and the average number of coronary plaques was approximately 0.4 in the control mice and 1.0 in the 16 Gy mice (11). Intriguingly, another study by Monceau et al. showed a significantly increase in cardiac fibrosis in ApoE$^{-/-}$ mice 40 weeks after 0.2 and 2 Gy focal heart irradiation. The authors also observed that focal heart irradiation of 0.2 Gy, but not 2 Gy, significantly decreased the survival of ApoE$^{-/-}$ mice (13). It would be interesting to conduct experiments that compare ApoE$^{-/-}$ mice exposed to various single doses of partial-heart vs. whole heart irradiation (for example, 0.2 to 16 Gy) to determine the radiation dose-volume effects in the heart.

In an autopsy series of patients treated with fractionated radiation therapy for Hodgkin Disease, there is evidence for radiation-induced obstructions of the coronary arteries (26). While no contemporary preclinical studies of cardiac irradiation have utilized conventionally fractionated doses, either in wild-type or ApoE$^{-/-}$ mice, a study by Hoving et al. did examine atherosclerosis following single and fractionated doses of neck irradiation in ApoE$^{-/-}$ mice and illustrated the effects of using clinically relevant fractionated doses (27). Hoving et al. used a single 8 or 14 Gy fraction or 2 Gy × 20 fractions to the neck, and found that while a single large fraction significantly increased total carotid artery plaque burden, there was no such increase after 2 Gy × 20 fractions. Specifically, while 2 Gy × 20 fractions to the neck initially increased the number of early plaques at 22 weeks, by 34 weeks there was no difference in the 2 Gy × 20 Gy mice and unirradiated control mice with respect to total, early, or advanced carotid artery plaques. While these experiments were carried out on the carotid, rather than the coronary arteries, the absence of significant late atherosclerosis in the mice receiving fractionated irradiation is intriguing and mirrors the

results of the present study. Together, these studies highlight the impact of dose-fractionation and assessment timepoints in studying atherosclerosis following radiation.

The major strengths of our study are the use the clinically relevant dose-fractionation and treatment volumes as well as the use of multimodality imaging to assess radiation-induced heart disease. Overall, our data reveal minimal late cardiac toxicity in wild-type mice and ApoE$^{-/-}$ mice on a regular diet following fractionated partial-heart RT when assessed by SPECT and echocardiography. Similarly, prior studies using SPECT did not show a significant change in myocardial perfusion in C57BL/6J mice after a single fraction of radiation to the entire heart and up to 30% of the bilateral lungs (10). However, our results suggest that more invasive assessment with PV loop analysis is more sensitive to detect changes in systolic and diastolic parameters in the ApoE$^{-/-}$ mice. Measurements taken by echocardiography and PV loop analysis had high correlation internally as expected, while correlation across modalities was less strong (Supplemental Figure 3). Thus, combining or comparing these modalities in future preclinical studies of RIHD are warranted.

There are several limitations of this study. First, unirradiated animals did not receive anesthesia 25 times with isoflurane as irradiated mice did during radiation treatment. It is conceivable that repeated exposure to isoflurane could potentially influence the phenotypes we observed due to transient effects of isoflurane on the cardiovascular system of mice (28–31). For example, one study indicated that C57BL/6J mice under isoflurane had a significant decrease in left ventricular systolic function compared to conscious mice by echocardiography (31). However, our echocardiogram data did not show a significant difference in left ventricular systolic function between unirradiated and irradiated C57BL/6J mice up to 18 months after isoflurane exposure. These results suggest that potential long-term effects of isoflurane on cardiac function, if any, would be less profound than the acute effects reported from mice during isoflurane treatment. Second, only female mice were used in the study because the goal of this project is to model cardiac injury from tangential field radiotherapy for breast cancer. Several clinical studies of childhood cancer survivors reveal a potential difference in the risk of cardiovascular diseases from genotoxic therapies based on biological sex (32–34). Notably, one recent pre-clinical study shows that female Dahl salt-sensitive/Mcwi rats developed more severe cardiotoxicity than age-matched male rats after a single dose of 24 Gy heart irradiation (35). Therefore, future investigations are warranted to compare cardiac injury after clinical-relevant partial-heart irradiation between male and female mice.

In conclusion, this study builds on prior RIHD studies by using more clinically relevant RT fields and dose-fractionation as well as a wide range of hemodynamic assessments. This novel pre-clinical model will be useful to study the contribution of other risk factors to the development of radiation-induced cardiovascular injury.

Supplementary Material

Refer to Web version on PubMed Central for supplementary material.

ACKNOWLEDGEMENTS

We thank Yi Qi for assisting with small animal imaging experiments and Mark Oldham for helping with dose-volume calculation. This work was supported by Susan G. Komen grant IIR13263571 (DGK), National Institutes of Health (NIH) National Cancer Institute grant R35CA197616 (DGK) and the Whitehead Scholar Award from Duke University School of Medicine (C-LL). SPECT, Dual energy micro-CT imaging and data analysis was performed at the Duke Center for In Vivo Microscopy and was supported by the NIH National Cancer Institute (R01 CA196667, U24 CA220245). Echocardiography and pressure-volume loop analysis were performed at the Duke Cardiovascular Physiology Core.

ABBREVIATIONS

RT	radiation therapy
ApoE$^{-/-}$	Apolipoprotein E-deficient
SPECT	Single-photon emission computed tomography
DE-CT	dual-energy microCT
PV	pressure-volume

REFERENCES

1. Cuzick J, Stewart H, Rutqvist L, Houghton J, Edwards R, Redmond C, et al.Cause-specific mortality in long-term survivors of breast cancer who participated in trials of radiotherapy. J Clin Oncol. 1994;12(3):447–53. [PubMed: 8120544]
2. Clarke M, Collins R, Darby S, Davies C, Elphinstone P, Evans V, et al.Effects of radiotherapy and of differences in the extent of surgery for early breast cancer on local recurrence and 15-year survival: an overview of the randomised trials. Lancet. 2005;366(9503):2087–106. [PubMed: 16360786]
3. Harris EE, Correa C, Hwang WT, Liao J, Litt HI, Ferrari VA, et al.Late cardiac mortality and morbidity in early-stage breast cancer patients after breast-conservation treatment. J Clin Oncol. 2006;24(25):4100–6. [PubMed: 16908933]
4. Darby SC, Ewertz M, McGale P, Bennet AM, Blom-Goldman U, Bronnum D, et al.Risk of ischemic heart disease in women after radiotherapy for breast cancer. N Engl J Med. 2013;368(11):987–98. [PubMed: 23484825]
5. Boerma M, Kruse JJ, van Loenen M, Klein HR, Bart CI, Zurcher C, et al.Increased deposition of von Willebrand factor in the rat heart after local ionizing irradiation. Strahlenther Onkol. 2004;180(2):109–16.
6. Boerma M, Wang J, Wondergem J, Joseph J, Qiu X, Kennedy RH, et al.Influence of mast cells on structural and functional manifestations of radiation-induced heart disease. Cancer Res. 2005;65(8):3100–7. [PubMed: 15833839]
7. Sridharan V, Aykin-Burns N, Tripathi P, Krager KJ, Sharma SK, Moros EG, et al.Radiation-induced alterations in mitochondria of the rat heart. Radiat Res. 2014;181(3):324–34. [PubMed: 24568130]
8. Boerma M, Singh P, Sridharan V, Tripathi P, Sharma S, Singh SP. Effects of Local Heart Irradiation in a Glutathione S-Transferase Alpha 4-Null Mouse Model. Radiat Res. 2015;183(6):610–9. [PubMed: 26010708]
9. Boerma M, Sridharan V, Mao XW, Nelson GA, Cheema AK, Koturbash I, et al.Effects of ionizing radiation on the heart. Mutat Res. 2016;770(Pt B):319–27.
10. Seemann I, Gabriels K, Visser NL, Hoving S, te Poele JA, Pol JF, et al.Irradiation induced modest changes in murine cardiac function despite progressive structural damage to the myocardium and microvasculature. Radiother Oncol. 2012;103(2):143–50. [PubMed: 22112779]
11. Gabriels K, Hoving S, Seemann I, Visser NL, Gijbels MJ, Pol JF, et al.Local heart irradiation of ApoE(−/−) mice induces microvascular and endocardial damage and accelerates coronary atherosclerosis. Radiother Oncol. 2012;105(3):358–64. [PubMed: 22959484]

12. Lee CL, Min H, Befera N, Clark D, Qi Y, Das S, et al.Assessing cardiac injury in mice with dual energy-microCT, 4D-microCT, and microSPECT imaging after partial heart irradiation. Int J Radiat Oncol Biol Phys. 2014;88(3):686–93. [PubMed: 24521682]
13. Monceau V, Meziani L, Strup-Perrot C, Morel E, Schmidt M, Haagen J, et al.Enhanced sensitivity to low dose irradiation of ApoE−/− mice mediated by early pro-inflammatory profile and delayed activation of the TGFbeta1 cascade involved in fibrogenesis. PLoS One. 2013;8(2):e57052. [PubMed: 23451141]
14. Lee CL, Moding EJ, Cuneo KC, Li Y, Sullivan JM, Mao L, et al.p53 functions in endothelial cells to prevent radiation-induced myocardial injury in mice. Sci Signal. 2012;5(234):ra52. [PubMed: 22827996]
15. Yoo B, Lemaire A, Mangmool S, Wolf MJ, Curcio A, Mao L, et al.Beta1-adrenergic receptors stimulate cardiac contractility and CaMKII activation in vivo and enhance cardiac dysfunction following myocardial infarction. Am J Physiol Heart Circ Physiol. 2009;297(4):H1377–86. [PubMed: 19633206]
16. Pacher P, Nagayama T, Mukhopadhyay P, Batkai S, Kass DA. Measurement of cardiac function using pressure-volume conductance catheter technique in mice and rats. Nat Protoc. 2008;3(9):1422–34. [PubMed: 18772869]
17. Abraham D, Mao L. Cardiac Pressure-Volume Loop Analysis Using Conductance Catheters in Mice. J Vis Exp. 2015(103).
18. Adams MJ, Hardenbergh PH, Constine LS, Lipshultz SE. Radiation-associated cardiovascular disease. Crit Rev Oncol Hematol. 2003;45(1):55–75. [PubMed: 12482572]
19. Clark DP, Holbrook M, Lee CL, Badea CT. Photon-counting cine-cardiac CT in the mouse. PLoS One. 2019;14(9):e0218417. [PubMed: 31536493]
20. Bhavane R, Badea C, Ghaghada KB, Clark D, Vela D, Moturu A, et al.Dual-energy computed tomography imaging of atherosclerotic plaques in a mouse model using a liposomal-iodine nanoparticle contrast agent. Circ Cardiovasc Imaging. 2013;6(2):285–94. [PubMed: 23349231]
21. Stewart JR, Fajardo LF, Gillette SM, Constine LS. Radiation injury to the heart. Int J Radiat Oncol Biol Phys. 1995;31(5):1205–11. [PubMed: 7713783]
22. Stone HB, Bernhard EJ, Coleman CN, Deye J, Capala J, Mitchell JB, et al.Preclinical Data on Efficacy of 10 Drug-Radiation Combinations: Evaluations, Concerns, and Recommendations. Transl Oncol. 2016;9(1):46–56. [PubMed: 26947881]
23. Sievert W, Trott KR, Azimzadeh O, Tapio S, Zitzelsberger H, Multhoff G. Late proliferating and inflammatory effects on murine microvascular heart and lung endothelial cells after irradiation. Radiother Oncol. 2015;117(2):376–81. [PubMed: 26233589]
24. Nakashima Y, Plump AS, Raines EW, Breslow JL, Ross R. ApoE-deficient mice develop lesions of all phases of atherosclerosis throughout the arterial tree. Arterioscler Thromb. 1994;14(1):133–40. [PubMed: 8274468]
25. Meir KS, Leitersdorf E. Atherosclerosis in the apolipoprotein-E-deficient mouse: a decade of progress. Arterioscler Thromb Vasc Biol. 2004;24(6):1006–14. [PubMed: 15087308]
26. Veinot JP, Edwards WD. Pathology of radiation-induced heart disease: a surgical and autopsy study of 27 cases. Hum Pathol. 1996;27(8):766–73. [PubMed: 8760008]
27. Hoving S, Heeneman S, Gijbels MJ, te Poele JA, Russell NS, Daemen MJ, et al.Single-dose and fractionated irradiation promote initiation and progression of atherosclerosis and induce an inflammatory plaque phenotype in ApoE(−/−) mice. Int J Radiat Oncol Biol Phys. 2008;71(3):848–57. [PubMed: 18514779]
28. Constantinides C, Murphy K. Molecular and Integrative Physiological Effects of Isoflurane Anesthesia: The Paradigm of Cardiovascular Studies in Rodents using Magnetic Resonance Imaging. Front Cardiovasc Med. 2016;3:23. [PubMed: 27525256]
29. Constantinides C, Mean R, Janssen BJ. Effects of isoflurane anesthesia on the cardiovascular function of the C57BL/6 mouse. ILAR J. 2011;52(3):e21–31. [PubMed: 21677360]
30. Roth DM, Swaney JS, Dalton ND, Gilpin EA, Ross J, Jr. Impact of anesthesia on cardiac function during echocardiography in mice. Am J Physiol Heart Circ Physiol. 2002;282(6):H2134–40. [PubMed: 12003821]

31. Pachon RE, Scharf BA, Vatner DE, Vatner SF. Best anesthetics for assessing left ventricular systolic function by echocardiography in mice. Am J Physiol Heart Circ Physiol. 2015;308(12):H1525–9. [PubMed: 25862835]

32. Armstrong GT, Sklar CA, Hudson MM, Robison LL. Long-term health status among survivors of childhood cancer: does sex matter?J Clin Oncol. 2007;25(28):4477–89. [PubMed: 17906209]

33. Bates JE, Howell RM, Liu Q, Yasui Y, Mulrooney DA, Dhakal S, et al.Therapy-Related Cardiac Risk in Childhood Cancer Survivors: An Analysis of the Childhood Cancer Survivor Study. J Clin Oncol. 2019;37(13):1090–101. [PubMed: 30860946]

34. Lipshultz SE, Lipsitz SR, Mone SM, Goorin AM, Sallan SE, Sanders SP, et al.Female sex and higher drug dose as risk factors for late cardiotoxic effects of doxorubicin therapy for childhood cancer. N Engl J Med. 1995;332(26):1738–43. [PubMed: 7760889]

35. Schlaak RA, Frei A, Schottstaedt AM, Tsaih SW, Fish BL, Harmann L, et al.Mapping genetic modifiers of radiation-induced cardiotoxicity to rat chromosome 3. Am J Physiol Heart Circ Physiol. 2019;316(6):H1267–H80. [PubMed: 30848680]

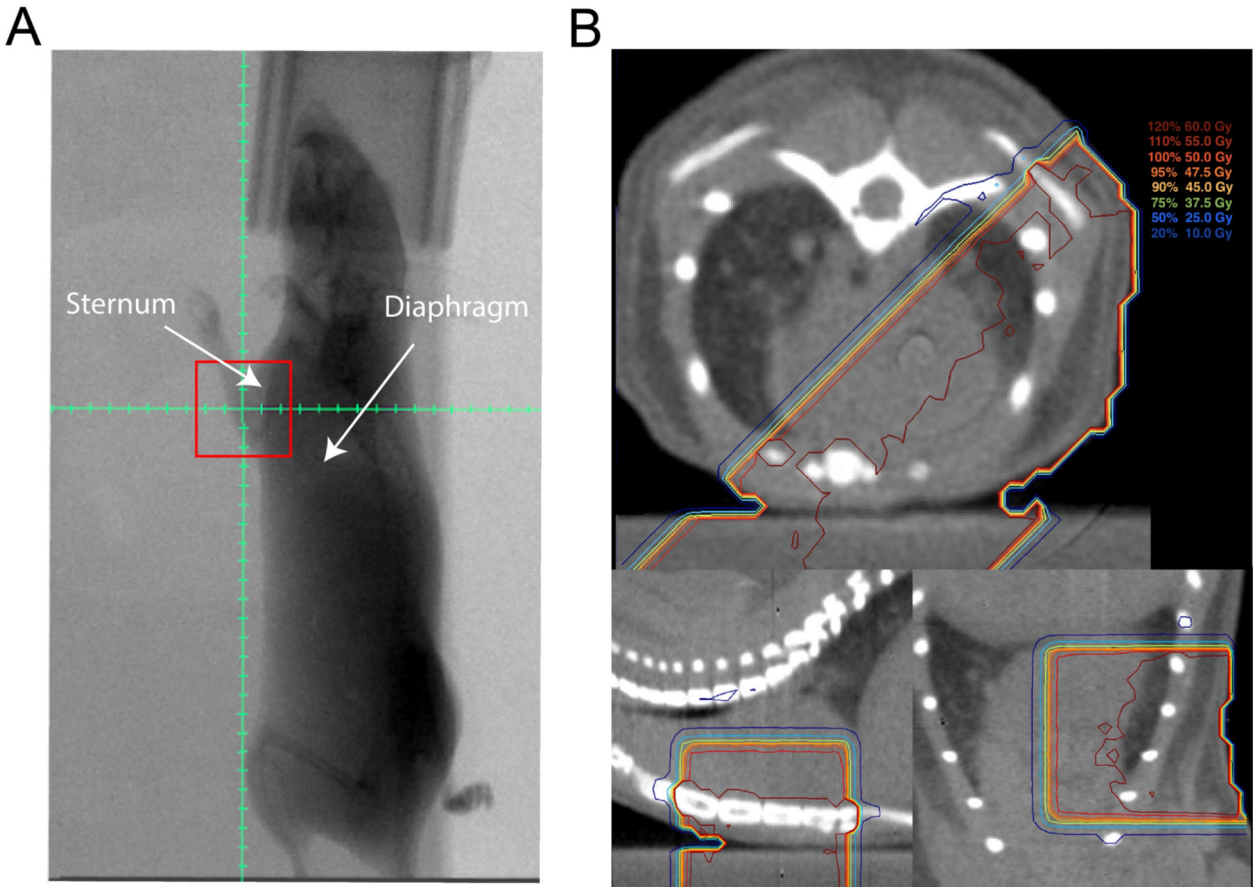

Figure 1.

Set-up and treatment plan for partial-heart radiation therapy. **(A)** Representative fluoroscopic image obtained at 315 degrees from right anterior oblique position with 10 × 10 mm treatment field (red square). Graticule with 2 mm tick marks shows isocenter, which was placed 2 mm anterior to sternum and 6–8 mm cranial to diaphragm. **(B)** Prescription isodose lines on a representative CT in the axial (top), sagittal (bottom left), and coronal (bottom right) planes showing prescription isodose lines covering part of the heart from opposed left posterior oblique and right anterior oblique treatment fields.

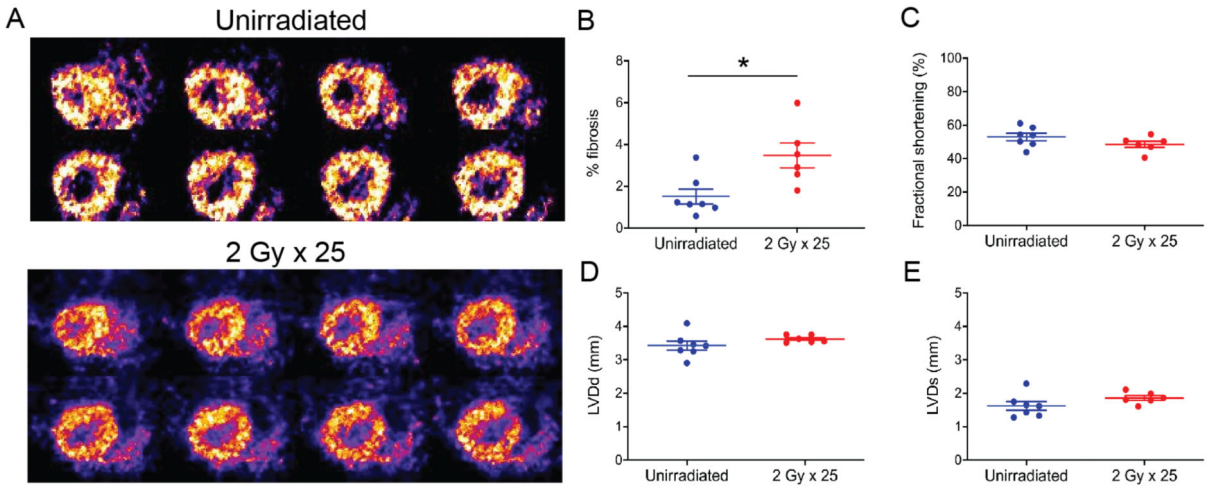

Figure 2.

Assessment of cardiovascular injury of C57BL/6J mice 18 months after irradiation. **(A)** Representative SPECT images of the heart after sham irradiation (n=7) or 2 Gy × 25 partial-heart irradiation (n=6). Mice were injected with 99mTc-tetrofosmin immediately before imaging. No substantial decrease in regional perfusion of the myocardium was observed in either unirradiated or irradiated mice. **(B)** Dot plot showing Sirius red staining of fibrosis in unirradiated (n=7) and irradiated (n=6) mice. (**C to E**) Echocardiography measurements of fractional shortening, left ventricular end diastolic diameter (LVDd) and end systolic diameter (LVDs) in unirradiated (n=7) and irradiated (n=6) mice. Each dot represents one mouse. Data are presented as mean ± SEM. *P<0.05 by Mann-Whitney U test.

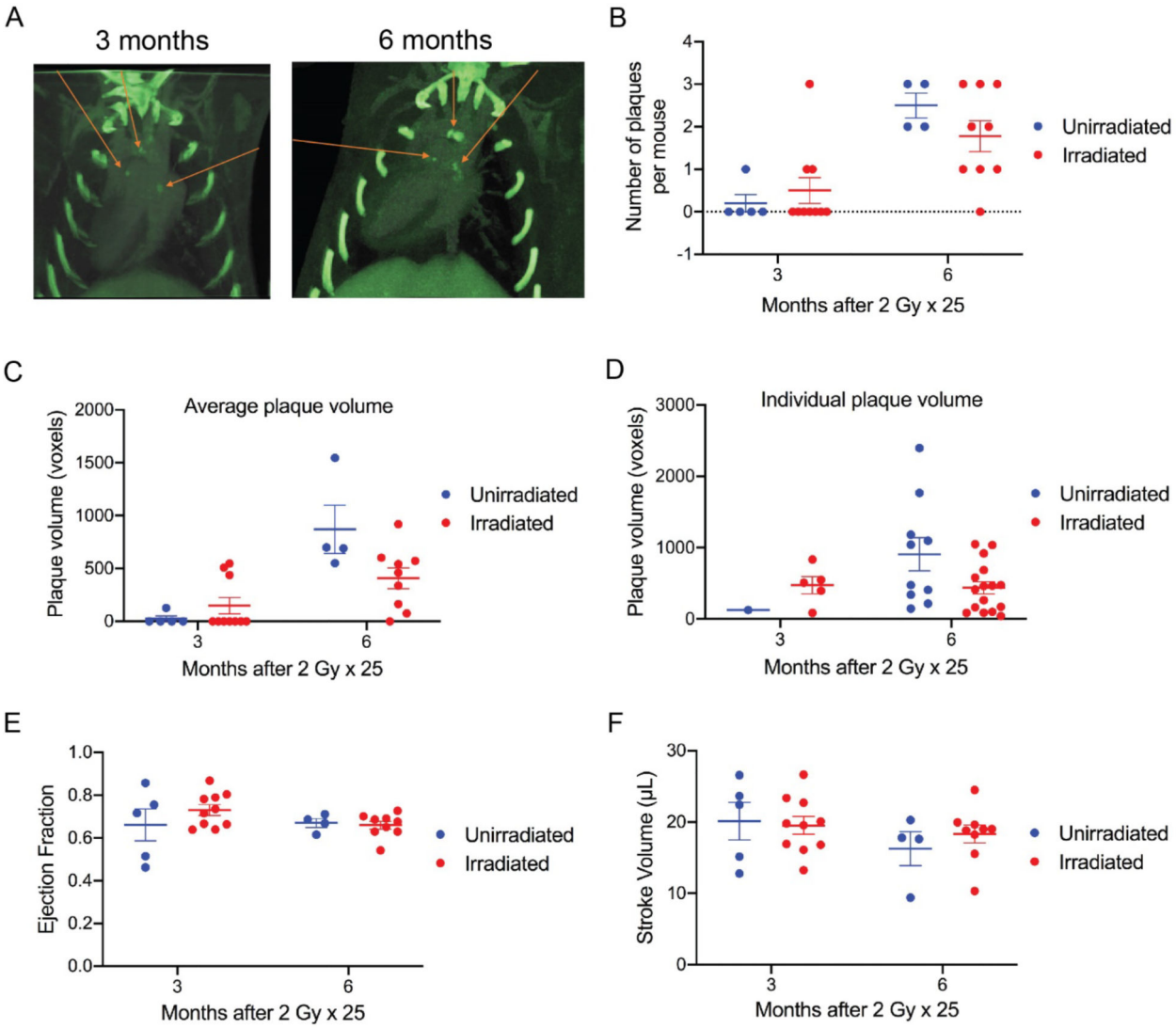

Figure 3.

Assessment of calcified plaques and cardiac function of irradiated and unirradiated ApoE$^{-/-}$ mice using dual-energy CT. **(A)** Representative images of calcified plaques detected by dual-energy CT. Images were obtained from the same mouse 3 and 6 months after 2 Gy × 25 partial-heart irradiation, respectively. Red arrow indicates individual plaques. **(B and C)** Dot plot showing the total number of calcified plaques and the average volume of plaques per mouse in unirradiated and irradiated mice 3 and 6 months after irradiation. Each dot represents one mouse. **(D)** Dot plot showing the volume of individual plaques per mouse in unirradiated and irradiated mice 3 and 6 months after irradiation. Each dot represents one plaque. **(E and F)** Assessment of ejection fraction and stroke volume by CT in unirradiated and irradiated mice 3 and 6 months after irradiation. Each dot represents one mouse. Data are presented as mean ± SEM. N=5 and 10 for unirradiated and irradiated mice, respectively, at 3 months; N=4 and 9 for unirradiated and irradiated mice, respectively, at 6 months. One unirradiated mouse was found dead after the 3-month scan and high-quality scan for one irradiated mouse at 6 months was not successfully acquired.

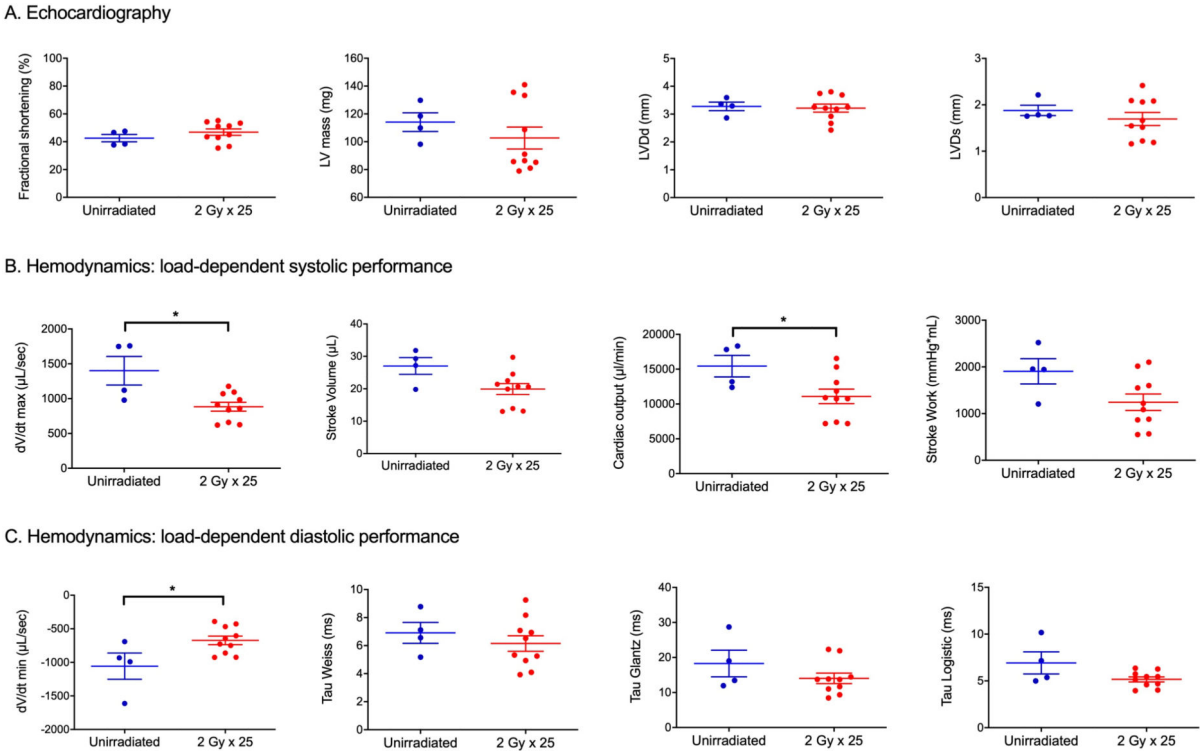

Figure 4.

Assessment of cardiac morphology and function of irradiated and unirradiated ApoE$^{-/-}$ mice using echocardiogram and pressure-volume loop analysis 12 months after irradiation. **(A)** Dot plot showing echocardiography measurements of fractional shortening, left ventricular (LV) mass, left ventricular end diastolic diameter (LVDd) and end systolic diameter (LVDs) in unirradiated (n=4) and irradiated (n=10) ApoE$^{-/-}$ mice. **(B)** Load-dependent LV systolic performance parameters derived from pressure-volume loop analysis of unirradiated (n=4) and irradiated (n=10) ApoE$^{-/-}$ mice. Each dot represents one mouse. **(C)** Load-dependent LV diastolic performance parameters derived from pressure-volume loop analysis of unirradiated (n=4) and irradiated (n=10) ApoE$^{-/-}$ mice. Each dot represents one mouse. Data are presented as mean ± SEM. *P<0.05 by Mann-Whitney U test.